



Nafion®/ODF-silica composite membranes for medium temperature proton exchange membrane fuel cells



Yaowapa Treekamol ^a, Mauricio Schieda ^{a,*}, Lucie Robitaille ^b, Sean M. MacKinnon ^b, Asmae Mokrini ^b, Zhiqing Shi ^c, Steven Holdcroft ^c, Karl Schulte ^d, Suzana P. Nunes ^e

^a Institute of Materials Research, Helmholtz-Zentrum Geesthacht, Max-Planck-Strasse 1, 21502 Geesthacht, Germany

^b NRC Industrial Materials Institute, 75 de Mortagne Boulevard, Boucherville, Quebec J4B 6Y4, Canada

^c Energy, Mining & Environment, National Research Council Canada, 4250 Wesbrook Mall, Vancouver, British Columbia V6T 1W5, Canada

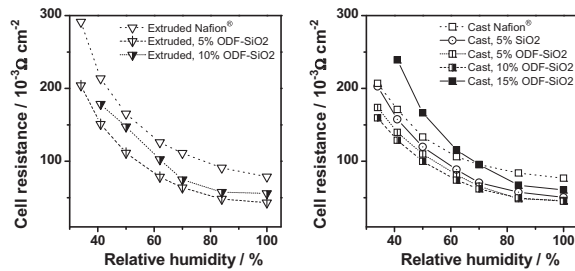
^d Institut M-11, Technische Universität Hamburg-Harburg, Denickestrasse 15, 21073 Hamburg, Germany

^e Water Desalination and Reuse Center, King Abdullah University of Science and Technology, Thuwal 23955-6900, Saudi Arabia

HIGHLIGHTS

- Compatibilized nanofillers result in improved fuel cell performance.
- Comparison of cast and melt-extruded Nafion® nanocomposites.
- Extensive study of influence of filler on membrane structure and properties.

GRAPHICAL ABSTRACT



ARTICLE INFO

Article history:

Received 25 July 2012

Received in revised form

5 January 2013

Accepted 18 January 2013

Available online 9 February 2013

Keywords:

Fuel cell
Polymer electrolyte membrane
Nafion
Nanocomposite
Functionalized silica

ABSTRACT

A series of composite membranes were prepared by dispersing fluorinated polyoxadiazole oligomer (ODF)-functionalized silica nanoparticles in a Nafion® matrix. Both melt-extrusion and solvent casting processes were explored. Ion exchange capacity, conductivity, water uptake and dimensional stability, thermal stability and morphology were characterized. The inclusion of functionalized nanoparticles proved advantageous, mainly due to a physical crosslinking effect and better water retention, with functionalized nanoparticles performing better than the pristine silica particles. For the same filler loading, better nanoparticle dispersion was achieved for solvent-cast membranes, resulting in higher proton conductivity. Filler agglomeration, however, was more severe for solvent-cast membranes at loadings beyond 5 wt.%. The composite membranes showed excellent thermal stability, allowing for operation in medium temperature PEM fuel cells. Fuel cell performance of the composite membranes decreases with decreasing relative humidity, but good performance values are still obtained at 34% RH and 90 °C, with the best results obtained for solvent cast membranes loaded with 10 wt.% ODF-functionalized silica. Hydrogen crossover of the composite membranes is higher than that for pure Nafion® membranes, possibly due to porosity resulting from suboptimal particle-matrix compatibility.

© 2013 Crown Copyright and Elsevier BV. All rights reserved.

1. Introduction

Fuel cells are highly versatile energy converters, but it is their relevance to automobiles in particular that has gathered

massive interest, especially after the advances made by companies like AFCC. Since proton exchange membrane fuel cells (PEMFCs) are the best suited for transport applications, an ever increasing number of research efforts have been directed towards the development of materials for this type of cells. Together with noble metal catalysts, the polymer electrolyte membranes [1–5] present a large number of challenges to

* Corresponding author. Tel.: +49 (0) 4152 87 24 82; fax: +49 (0) 4152 87 4 24 82.

E-mail address: mauricio.schieda@hzg.de (M. Schieda).

commercialization, mainly due to their cost, durability, and limited operating range.

Several advantages are ascribed to the operation of PEMFCs at medium to high temperatures (>100 °C), including improved electrochemical kinetics, simpler water management and cooling, and waste heat recovery [6]. Furthermore, cost reduction requires the elimination of humidifier systems, which implies fuel cell operation at low relative humidity (RH). While perfluorosulfonic acid (PFSA) polymers such as Nafion® are still the standard solid electrolyte employed in commercial PEMFCs, their performance decreases rapidly at high temperatures and low RH, as the membrane dehydrates [7–10]. Hence the development of new membrane materials with properties suited to high temperature and low humidity operation remains one of the pressing issues towards wide commercialization of PEMFCs.

The two main research approaches are the development of new polymers, with structures designed in a bottom-up fashion, or the modification of previously known polymers, by functionalization, blending or composite formulation. A number of reviews have been recently published on the preparation of hybrid inorganic–organic composite membranes for fuel cell applications [11–19]. Widely explored strategies consist of introducing clay [20,21], layered metal phosphates and phosphonates [22], or hydrophilic oxides [23–25] (MO₂, with M = Si, Ti, Zr, Sn) in a conducting polymer matrix, either by simple dispersion or by *in-situ* generation via sol–gel process. In all cases the aim is to limit the rate of dehydration and the reactant permeability of the polymer electrolyte matrix.

Several groups have investigated the preparation of poly-electrolyte composite membranes containing sol–gel *in-situ*-generated SiO₂ [26–29]. However, because of its wide availability and low cost, the simplest approach is still the dispersion of silica particles as filler in a conducting polymer matrix. Previous studies have demonstrated the advantage of employing functionalized silica compared to neat silica [30,31], and of nanoparticles versus larger particles [32].

In this study we report the preparation of Nafion® composite membranes containing polyoxadiazole (POD) functionalized silica nanoparticles, and presenting higher performance in fuel cells operating at medium temperatures and low relative humidity. As a grafting agent we have used sulfonated, fluorinated polyoxadiazole oligomers (ODF), which provide a good interaction with both the hydrophobic and the hydrophilic phases of Nafion®, and compensate for the dilution of ion exchange functions by adding protogenic species, in the form of $-\text{SO}_3\text{H}$ groups, and protonable moieties, in the form of oxadiazole rings [33–35]. We compare membranes prepared by solution casting and melt-extrusion.

2. Experimental

2.1. Materials

Nafion® perfluorinated resin solution (5 wt.% in lower aliphatic alcohols and water), hydrazine sulphate (99%), 4-fluorobenzoic acid (98%), sodium hydrogen carbonate (99%), potassium carbonate (99%), N,N-dimethylacetamide (DMAc) (99.9%), dimethylsulfoxide (DMSO) (99.5%), sulphuric acid (95–97%) and poly(phosphoric acid) (PPA) (115% H₃PO₄ basis) were acquired from Sigma–Aldrich. Ethanol (99.9%), methanol (99.9%), N-methyl-2-pyrrolidone (NMP) (99.5%), toluene (99.9%, Merck), were obtained from Merck. Bro-mophenyltrimethoxysilane (mixed isomers) was acquired from Gelest. Nafion® perfluorosulfonic acid (PFSA) resin R-1000 (DuPont) was obtained from Ion Power Inc., fumed silica Aerosil 380 (7 nm, 380 m² g⁻¹) was acquired from Evonik. Carbon paper (Sigracet SGL-24BC) was supplied by SGL Carbon SE. All chemicals were used as received.

2.2. Functionalization of silica nanoparticles

Silica nanoparticles were functionalized by reaction with bro-mophenyltrimethoxysilane and further grafting with a fluorinated aromatic bishydroxy terminated oligomer containing oxadiazole groups. Detailed descriptions of the oligomer synthesis and the particle functionalization procedure can be found elsewhere [36,37]. The oligomer used in this work is a poly(hexafluoroisopropylidene-diphenyl-co-1,3,4-oxadiazole–diphenylether) (ODF). After functionalization, the particles contained 0.23 mmol ODF per gram of silica, corresponding to a 53 ± 2% grafted mass, as determined by TGA. We will refer to the functionalized silica as “ODF-silica”, or simply “ODF-SiO₂”, in the following paragraphs.

2.3. Membrane fabrication

2.3.1. Solvent-cast Nafion® composites

A 5 wt.% Nafion® solution was employed in the preparation of the functionalized silica-Nafion® composite membranes. Since the oligomers attached to the silica surface have a good solubility in DMAc, this solvent was added in a ratio 2:1 to the Nafion® solution in order to improve the nanoparticle dispersion. After that, functionalized silica was added to the mixture. The solutions were then vigorously stirred for 4 h at 50 °C so as to partially evaporate the solvent mixture until a 10 wt.% Nafion® solution was obtained. Subsequently the mixtures were stirred overnight and sonicated for 30 min to disperse the silica particles. Finally, a doctor blade with a 650 µm gap was used to cast the solutions on clean glass plates. The cast membranes were kept at 60 °C overnight and then cooled down to room temperature. Finally, the films were detached from the glass plates, and dried in a vacuum oven at 60 °C overnight. The thickness of the resulting membranes was around 30–40 µm.

2.3.2. Melt-extruded Nafion® composites

Blends based on extrusion grade Nafion® in the sulfonyl fluoride (–SO₂F) form [38] containing 5 and 10 wt.% of functionalized silica were prepared in a 5 cm³ DSM micro-twin screw extruder at 240 °C (above 10 wt.% the melts were too viscous for our extruder configuration). A two-step extrusion process was applied: nanocomposite blend preparation using counter-rotation screws configuration, followed by film preparation using co-rotation screws configuration. A screw rotation speed ranging from 5 to 10.5 rad s⁻¹ (~50–100 rpm) was used. The extruder was equipped with a 0.1 mm × 3.5 cm die. The thickness of the resulting membranes was in the range 25–35 µm.

The blends containing 10 wt.% silica particles had a high viscosity, resulting in less uniform films when compared to the 5 wt.% blends. Nafion in the sulfonyl fluoride form does not have cation-exchange properties and must be chemically treated to make it suitable for use in applications requiring proton conduction. The extruded Nafion® film was converted to the salt (K⁺) and acid (H⁺) forms following a process similar to the one recommended by the manufacturer [39]. The film was hydrolysed by immersion in a solution of 10% potassium hydroxide, 37% DMSO and 53% de-ionized (DI) water at 40 °C for 30 min. Subsequently, the film was thoroughly washed with DI water, by soaking three times in room-temperature DI water for 30 min, in order to remove all traces of unreacted KOH. Finally the membrane was dried in vacuum oven at 60 °C for 12 h. The hydrolysed film was changed to the H⁺ form by exchanging the K⁺ for H⁺ ions in a 15% solution of nitric acid (HNO₃). This step was repeated three times with fresh nitric acid, including a fresh DI water rinse after each acid treatment. After that, the film was immersed three times in room-temperature DI water for 30 min. Finally the membrane was dried out in vacuum oven at 60 °C for 12 h.

2.3.3. In-situ post-sulphonation of the functionalized filler

In order to attach sulfonic acid groups onto the telechelic chains grafted on the silica nanoparticles, the Nafion® composite membranes were subjected to a post-sulphonation treatment, by soaking the membranes in 50 wt.% H₂SO₄ at room temperature overnight. After that, the residual acid was washed out by rinsing the membranes with fresh DI water and then immersing them in fresh DI water for 30 min. The washing procedure was repeated several times, checking the wash water with pH paper strips, until a pH ~7 was obtained. Finally, the membranes were dried at 60 °C overnight in vacuum oven. The pure Nafion® membranes were subjected to the same treatment in order to have comparable conditioning across the whole series of samples.

2.4. Membrane characterization

2.4.1. Water uptake measurement and thickness expansion

For the water uptake characterization, the films were fully hydrated by immersion for 2 days in DI water at room temperature. The water-saturated membrane samples were weighed after quickly wiping the excess water with residue-free tissue paper. The samples were then placed in the vacuum oven at 80 °C overnight to remove the absorbed water. After cooling down to room temperature, the weight of the dry membranes was measured. The mass-based water uptake (WUm) was calculated with the equation:

$$WUm(\%) = \frac{m_{\text{wet}} - m_{\text{dry}}}{m_{\text{dry}}} \times 100\%$$

where m_{dry} and m_{wet} are the masses of dry and wet samples, respectively.

The swelling ratio (Δt) of the membranes was calculated by measuring the thickness of the membranes before and after the water uptake measurement, according to the equation:

$$\Delta t(\%) = \frac{t_{\text{wet}} - t_{\text{dry}}}{t_{\text{dry}}} \times 100\%$$

where t_{dry} and t_{wet} are the thickness of the dried and wet samples, respectively.

2.4.2. Ion exchange capacity

For the determination of the ion exchange capacity, the films in H⁺ form were first equilibrated for 48 h in 0.2 M NaCl at room temperature with regular agitation. The equilibration baths were then titrated with NaOH (0.005 M) with a Metler Toledo T50 automatic titrator. The procedure was carried out three times and the results averaged.

2.4.3. Ionic conductivity

Through-plane ionic conductivity was measured by electrochemical impedance spectroscopy (EIS), at room temperature and 100% relative humidity. Using an HP4192A impedance analyzer, the frequency scan was carried out from 50 Hz to 5 MHz with an AC perturbing signal amplitude of 0.1 V. Pure polymer membrane samples were measured as a reference before each series of measurements. The resistivity of the membrane was obtained from the high frequency part of the Nyquist plot, corresponding to the bulk resistance of the polymer. Ionic conductivity of the samples was calculated using the equation:

$$\sigma = \frac{1}{R_{\text{bulk}}} \times \frac{d}{A}$$

where σ is the conductivity, d is the distance between electrodes, A is the contact area between the electrodes and the polymer film,

and R_{bulk} is the bulk resistance obtained from Nyquist plot of the impedance spectrum.

2.4.4. Thermal analysis

The thermal stability of polymer composite membranes was determined by thermogravimetric analysis (TGA) in a Netzsch TG 209 F1 Iris thermo-microbalance. The temperature was scanned in the range 25–800 °C, with a heating rate of 10 °C min⁻¹, under argon sweep (for the determination of grafted mass: 5 °C min⁻¹ and air sweep). Differential scanning calorimetry (DSC) measurements were carried out in a Netzsch DSC 204 Phoenix® calorimeter. A mass of 8–20 mg of sample was introduced in an aluminium pan with a perforated cover, and a preliminary DSC run at 10 °C min⁻¹, from 25 to 150 °C, was employed on all samples to eliminate adsorbed water. The sample was subsequently cooled down to –150 °C at 30 °C min⁻¹, and finally a dynamic run at 10 °C min⁻¹ was performed up to 280 °C. An empty aluminium pan was used as reference. For the analysis of volatile thermal degradation products in inert atmosphere, a Bruker Equinox 55 infrared spectrometer was employed, connected through a Bruker TGA-FTIR interface to a Netzsch TG 209 thermo-microbalance. The thermograms were recorded at 10 °C min⁻¹, and argon was used as sweep gas to transfer the gaseous products of thermal degradation through heated PTFE tubing into a heated 8.7 mL cell in the spectrometer interface.

2.5. Fuel cell performance evaluation

The gas diffusion electrodes (GDEs) were prepared by auto-spraying a homogeneous catalyst ink, consisting of carbon powder-supported platinum (Pt), Nafion® solution, and isopropanol onto a gas diffusion layer (GDL). The GDL consists of PTFE-treated carbon paper (SGL-24BC), impregnated with a PTFE and carbon black microporous layer (MPL). The total Pt loading for both anode and cathode was 0.4 mg Pt cm⁻². The total Nafion® loading in the catalyst layer (CL) was 30%. The 5 cm² area membrane electrode assemblies (MEAs) were prepared by hot pressing the anode GDE, Nafion® composite membrane, and the cathode GDE together at 135 °C at ~4 MPa for 3 min. Then the MEA was cooled down under constant pressure to 30 °C for 5 min. Both bipolar plates had identical serpentine flow fields with a nominal area of 5 cm². The depth and width of the channels and the width of the ribs on the flow fields were all 0.84 mm.

The MEA was tested in a Teledyne 125 W test station under atmospheric pressure, with relative humidity (RH) ranging from 34 to 100%. Before the test, the cell was conditioned by drawing current at 0.6 V for 12 h, in order to activate the electrochemical reaction sites in the catalyst layers of both anode and cathode. Afterwards, polarization data were collected as a function of RH, by varying the cell temperature, and keeping the saturator temperature constant at 64 °C. The resulting temperature–humidity pairs are shown in Table S1, in the Supplementary Materials. Cell voltage and cell resistance were recorded as a function of RH under a 1 A cm⁻² current density after 1 h stabilization at the same load. The gas streams of pure H₂ and O₂ were controlled by their respective mass flow controllers and the flow rates were kept at 0.2 L min⁻¹ (at standard conditions of 1 atm and 25 °C). Before H₂ and O₂ were fed into the anode and cathode, they were humidified by passing through their corresponding humidifiers at 64 °C.

2.5.1. Hydrogen crossover measurement

In order to measure the H₂ crossover, an MEA was assembled into a cell and conditioned for 12 h under load at 0.6 V and 100% RH. After that the load was removed, and a humidified N₂ stream at

1 L min⁻¹ was applied to the cathode side to purge any oxygen traces. Once a stable cell voltage was obtained (~ 0.1 V), the N₂ flow rate was changed back to 0.2 L min⁻¹. Then a Solartron 1287 potentiostat was connected to the fuel cell, with the working electrode probe joined to the cathode, and the counter/reference electrode probes connected to the anode. CorrWare software was used to apply four potential steps in the range 0.2–0.5 V, and record the corresponding current values after stabilization (about 15 min). In this potential range, all H₂ that has crossed over from the anode to the cathode should be completely oxidized, giving a current indicative of the amount of H₂ that has crossed over. The reported crossover value is obtained from extrapolation to open circuit potential [8].

3. Results and discussion

3.1. Morphological analysis

SEM micrographs of the composite membranes are shown in Fig. 3. Filler agglomeration in the solvent-cast membranes is already observable at 10 wt.% loading, and significant at 15 wt.%. Solvent-cast membranes show a number of macroaggregates, the largest of which tend to accumulate towards the bottom side of the membrane. Nevertheless, a significant fraction of filler is still distributed in well-dispersed very small aggregates. Conversely, extruded membranes present a large number of evenly distributed medium-size agglomerates.

3.2. Electrochemical characterization

The main function of the polymer electrolyte membrane in a fuel cell is proton transport. In sulfonic acid based membranes, the proton conductivity depends on the amount of accessible acid groups and their dissociation potential in water [40]. Thus, ion exchange capacity and conductivity can provide insight into the ability of a membrane to transport protons.

Fig. 1 shows IEC values for the Nafion® composite membranes as a function of filler content. For solvent-cast membranes, introducing 5 wt.% of silica nanoparticles causes a reduction in the IEC: from 0.91 down to 0.80 meq g⁻¹ for neat silica, and a slightly lower decrease for functionalized silica, down to 0.82 meq g⁻¹. However,

for membranes containing 10 wt.% of functionalized filler, the IEC stabilizes, even slightly increasing back from 0.81 to 0.84 meq g⁻¹, as the sulfonic acid groups in the oligomers compensate for the loss of sulfonated matrix. This is in contrast with 10 wt.% neat silica composites, for which the IEC continues to decrease down to 0.73 meq g⁻¹. Nevertheless, with a further increase in the loading of functionalized silica to 15 wt.%, the IEC drops down again, probably due to the agglomeration of filler particles, which makes a large portion of the oligomer-bonded sulfonic acid groups inaccessible. A similar trend is found for the extruded, functionalized-silica composite membranes. IEC decreases to 0.85 meq g⁻¹ for 5 wt.% loading, but stabilizes and slightly increases back to 0.88 meq g⁻¹ for films with 10 wt.% filler content.

The through-plane conductivities of solvent-cast and extruded composite membranes with increasing loadings are shown in Fig. 2. For our solvent-cast pure Nafion® membranes, the conductivity was around 56 mS cm⁻¹ 5 wt.% loadings of neat and functionalized silica reduce this value to 24 and 36 mS cm⁻¹ respectively. For the 10 wt.% composites, the proton conductivity increases again to 49 mS cm⁻¹ for functionalized silica particles, but continues to drop for membranes with neat silica.

The dependency of conductivity values on filler type and content is similar to the trend observed for IEC values. The presence of sulfonate groups on the ODF-functionalized silica compensates for the loss of sulfonated polymer matrix [31]. Furthermore, the oxadiazole groups contain a basic nitrogen ($-N=$) which can contribute to the charge transport by exchanging protons with sulfonic acid groups ($-SO_3H$) [34]. The decline in conductivity towards 15 wt.% grafted silica content can be similarly explained by nanoparticle agglomeration, with the consequent loss of sulfonate group accessibility.

The average IEC values for the ODF-silica composites prepared by solvent casting are similar to the values for the extruded membranes. However, higher proton conductivity values are observed for solvent-cast membranes when compared to extruded membranes with the same filler content. A possible explanation is the better dispersion achieved in the solvent-cast membranes, as shown by the SEM micrographs in Fig. 3. While proton-exchange groups in the core of moderately size agglomerates are still accessible for ion exchange, and thus contribute to the global IEC of the membrane, only the groups on the agglomerate surface, in intimate contact with

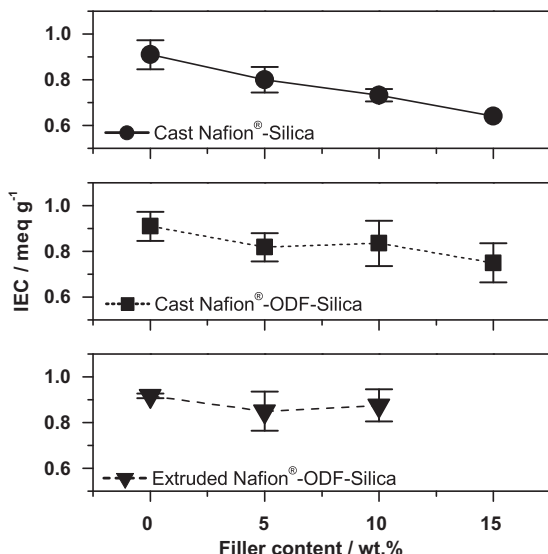


Fig. 1. Ion exchange capacity of Nafion® composite membranes as a function of filler content.

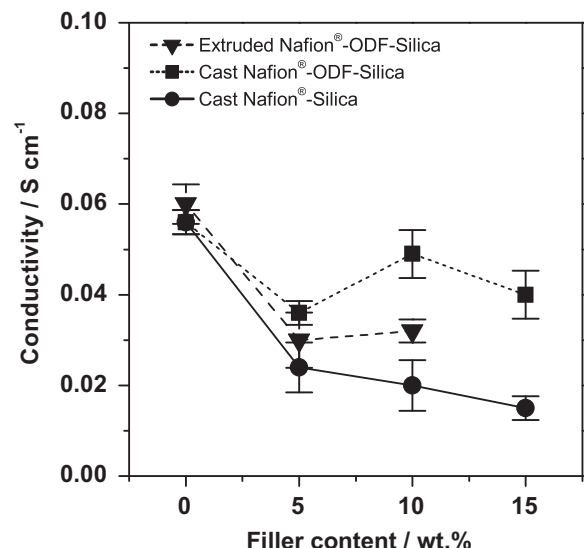


Fig. 2. Proton conductivity of the Nafion® composite membranes as a function of filler content.

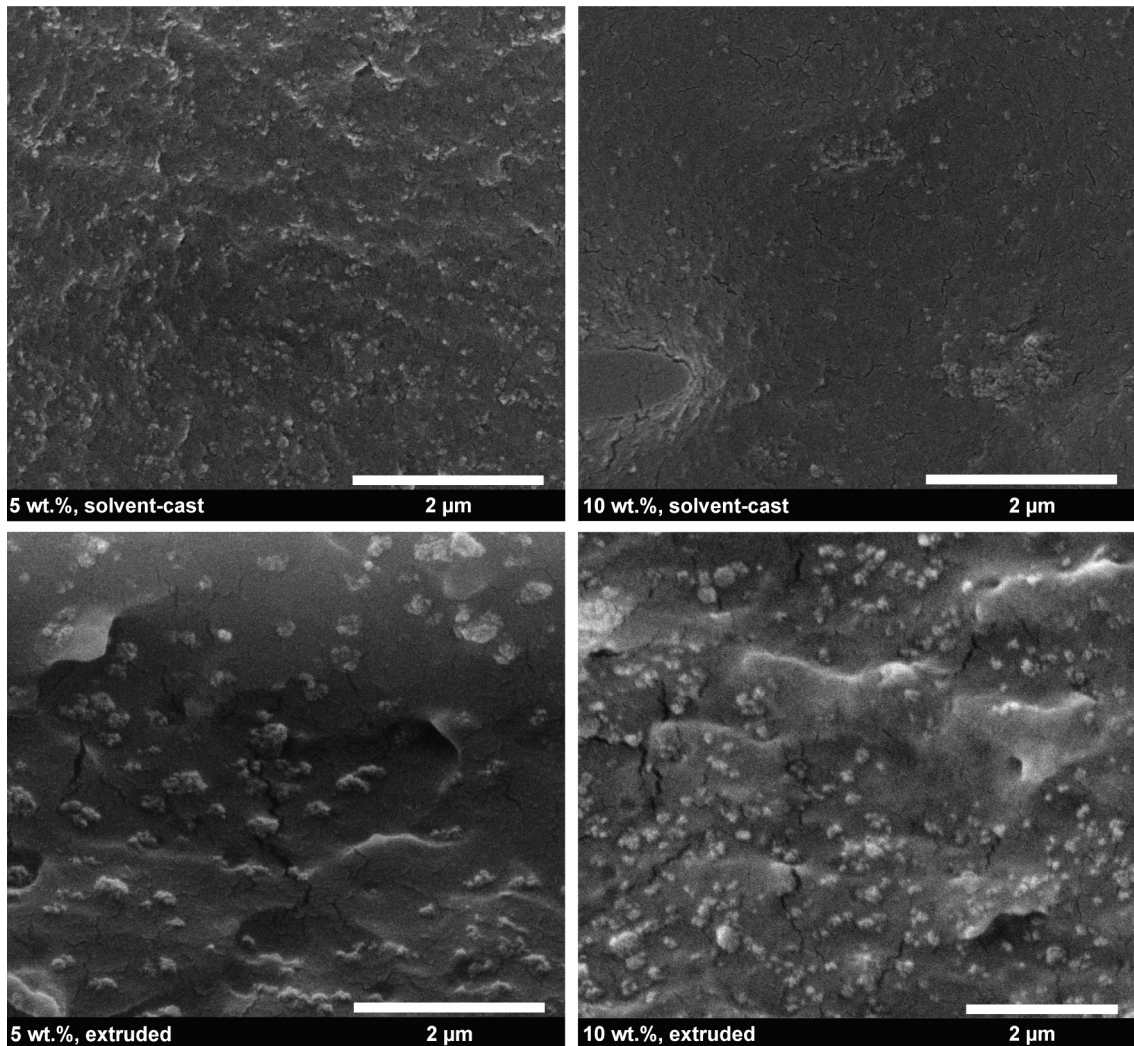


Fig. 3. SEM micrographs of 5 and 10 wt.% solvent-cast (top) and 5 and 10 wt.% extruded (bottom) Nafion® composite membranes containing ODF-functionalized silica nanoparticles. Micrographs obtained at 10–25 kV beam voltage (ETD detector), in order to increase the visibility of the smaller aggregates. The small cracks are due to beam damage.

the protogenic matrix, contribute significantly to the proton conductivity of the composite.

3.3. Water uptake and thickness expansion

Figs. 4 and 5 show respectively the evolution of water uptake and of thickness expansion, at room temperature and 100% RH, for Nafion® composite membranes with increasing filler contents.

For solvent-cast ODF-functionalized silica composites, water uptake drops from the 58% of pure Nafion® down to 35% for membranes containing 5 wt.% of filler. For higher filler contents the water uptake slowly increases up to 42% for membranes with 15 wt.% loading. While a similar trend is observed for the solvent-cast composites containing neat-silica, the latter presents higher water uptakes at all loadings (down to 43, and then up again to 50 and 57%, for composites with loadings of 5, 10 and 15 wt.% respectively).

A probable explanation for the initial drop in water uptake is the reinforcement effect of the particulate fillers. The nanoparticles act as physical crosslinks, significantly reducing swelling. As filler aggregation increases for the composites with higher loadings, the specific surface area of the fillers is reduced, and consequently the interaction with the matrix is less effective. Additionally, the ODF-functionalized silica particles contribute to the water uptake as

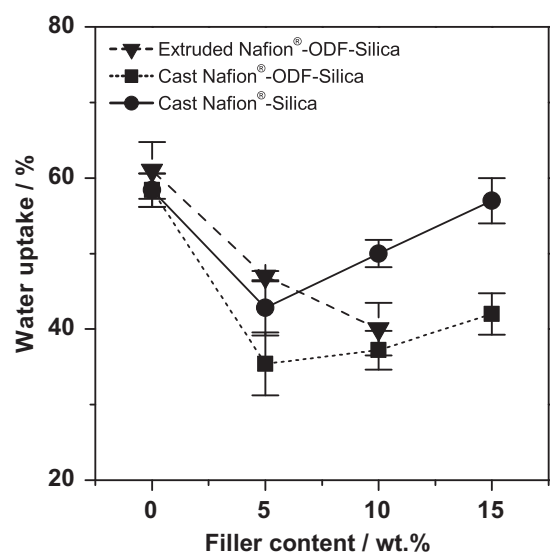


Fig. 4. Water uptake at room temperature and 100% RH for Nafion® and composite membranes as a function of filler content.

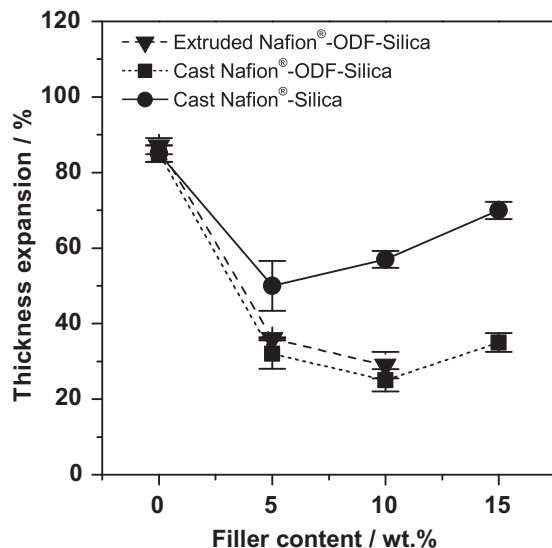


Fig. 5. Thickness expansion at room temperature and 100% RH for Nafion® and composites as a function of filler content.

they carry sulfonic acid groups. The drop in water uptake is less marked in the extruded membranes, as agglomeration is significant already at 5 wt.% loading.

Compared to the ODF-functionalized silica, the neat-silica particles have a lower affinity for the perfluorinated matrix. This originates a lower initial decrease in water uptake for the 5 wt.% neat-silica composites, and also in a faster increment in water uptake at higher filler contents, as agglomeration increases, and the interaction with the matrix is less efficient.

Analogously, for ODF-functionalized silica composites, both solvent-cast and extruded, the thickness expansion (Fig. 5) drops from ~85% for pure Nafion®, down to ~35% for the membranes with 5 wt.% filler content, and remains relatively stable at higher contents. This is in agreement with a strong interaction between the particles and the matrix. In contrast, for the neat-silica composites, with a weaker matrix–particle interaction, the thickness expansion increases again at higher loadings, as particle aggregation reduces the specific area of the fillers.

The water uptake values obtained are relatively high. This can be explained by the conditioning protocol: all these membranes were subjected to the same post-sulphonation treatment described in Section 2.3.3, in order to in-situ sulfonate the functionalized fillers (in the case of the pure polymers, the sulphonation was also carried out in order to have the same conditioning for all membranes).

The thickness expansion values obtained are also rather high. For example, for pure Nafion® (0 wt. % in Figs. 4 and 5) the theoretical isotropic expansion coefficients ($\Delta t = [((mH_2O^*\rho_{Poly}/mPoly^*\rho_{H_2O}) + 1)^{(1/3)}] - 1$), would be around ~30%, less than half the experimental values reported in Fig. 5. These high values could be explained by anisotropic expansion, due to uniaxial orientation introduced by our membrane preparation techniques.

3.4. Thermal analysis

3.4.1. TGA

Thermogravimetric analysis curves for composite membranes studied in this work are shown in Fig. 6. The mass residues after each thermal decomposition step, as well as the temperatures of the maxima of the derivative curves (DTG) for relevant steps, are given in Table 1 for solvent-cast and extruded Nafion® composites.

An initial mass loss (I) in the range 25–180 °C (not shown in the figure), with a derivative maximum around 120 °C, can be attributed to the elimination of adsorbed water, most of which is adsorbed in the ionic clusters of the Nafion® matrix [41].

The second mass loss step (II), in range of 300–400 °C, with DTG maximum in the range 340–380 °C, corresponds to the partial loss of sulfonic acid groups [42,43]. A net tendency is observed for the composites, with a shift of the DTG maximum to lower temperatures, as the content of grafted silica increases, probably due to contribution from the degradation of filler particles. However, the total mass loss is significantly lower in this step for the highly loaded composites. Three phenomena may account for this effect: firstly, at high filler loadings, the amount of Nafion® sulfonic acid groups is lower due to the decreasing fraction of polymeric matrix in the composite. Secondly, while the matrix-bonded $-SO_3H$ groups might, as they decompose, catalyse the degradation of the filler nanoparticles exposed to the matrix, at high loadings, due to agglomeration, a significant amount of filler

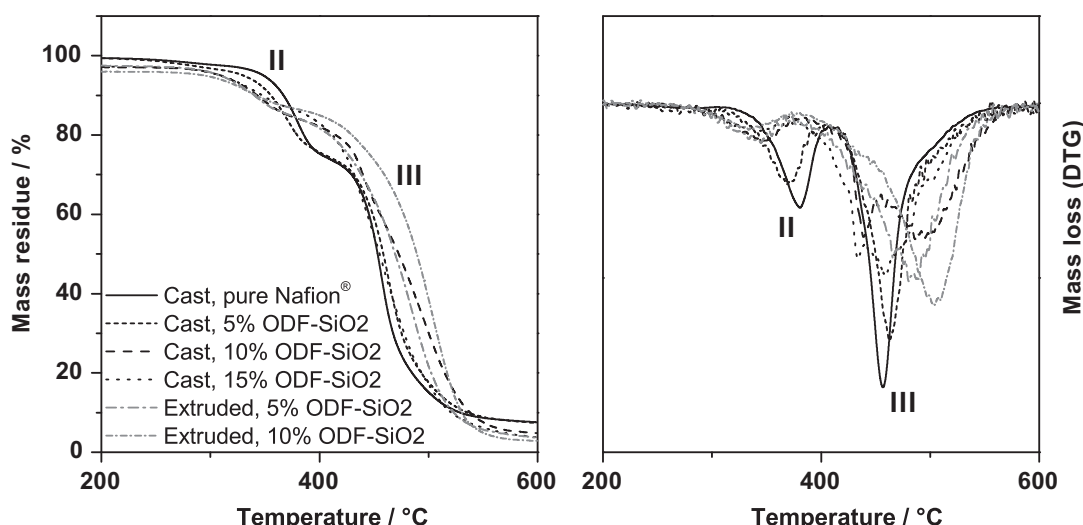


Fig. 6. TGA curves obtained for solvent-cast and extruded Nafion® composites studied in this work. The derivative curves (DTG) are shown on the right side. See the text for a description of the mass loss step nomenclature.

Table 1

Mass loss for each of the three main steps in the thermograms of Nafion® ODF-silica composite membranes. The temperatures of the DTG maxima for the decomposition steps (II and III) are also reported.

Membranes	Mass loss/%			Temperatures of DTG maxima/°C	
	I	II	III	II	III
Cast Nafion®	0.58	25.30	69.60	380.4	455.9
Cast Nafion®, 5% ODF-SiO ₂	0.50	24.28	70.22	370.2	463.4
Cast Nafion®, 10% ODF-SiO ₂	2.84	13.04	80.93	348.9	439.7; 493.2
Cast Nafion®, 15% ODF-SiO ₂	2.77	10.07	84.23	344.4	432.8; 460.2 ^a
Extruded Nafion®, 5% ODF-SiO ₂	2.50	11.87	83.38	341.8	484.8
Extruded Nafion®, 10% ODF-SiO ₂	4.01	9.35	86.21	334.9	503.7

^a Shoulder at 504.2.

is “protected” inside the agglomerates, and only contributes to mass loss at higher temperatures. Finally, on average, the $-\text{SO}_3\text{H}$ groups present higher thermal stability, and decompose at higher temperatures, mainly due to the limitation on side chain mobility caused by the dispersed ODF-SiO₂ nanoparticles. A similar stability increase in the matrix $-\text{SO}_3\text{H}$ groups was observed by Deng et al. [44] for Nafion® composites containing *in-situ* generated, post-functionalized SiO₂.

The third mass loss step (III), ranging from 420 to 550 °C, consists of the complete oxidative degradation of the C–O–C moieties along with the fluorocarbon backbone in Nafion®, and of any remaining sulfonic acid groups [42,45]. The derivative of the thermogram evidences two stages for this step, with maxima in the ranges 430–470 (IIIa) and 480–520 (IIIb). For the composites, these last steps also include the degradation of the grafted oligomer backbone that is not in direct contact with the Nafion® matrix, which occurs in two consecutive steps as well, with DTG maxima at 515 °C and 540 °C.

3.4.2. TGA-FTIR

Infrared analysis of the gases evolved during thermal decomposition provides further information regarding the effect of the ODF-SiO₂ particles on the structure and thermal stability of

Nafion®. For solvent-cast pure Nafion®, telechelic oligomer ODF (post-sulfonated *ex-situ* with the same protocol applied to the composites and described earlier), and for the solvent-cast composite with 10 wt.% ODF-SiO₂, a series of FTIR spectra were obtained, at constant temperature intervals, from the volatile products generated during thermogravimetric runs in inert atmosphere. The thermograms were carried out on dry membranes, with an initial 15 min isotherm at 110 °C performed in order to further eliminate adsorbed water. Fig. S1 in the Supplementary Materials shows the resulting spectra at 335, 440, 485 and 530 °C.

For both pure cast Nafion® and its composite, the most significant absorption bands correspond to SO₂ (1330 cm⁻¹), and SiF₄/CF₃CFCF₂ (1022 cm⁻¹) in agreement with previous observations on SiO₂-Nafion® composites [44]. Both decompose to give gaseous mixtures with medium to strong absorptions for CO₂ (2320–2360 cm⁻¹) and substituted carbonyl fluorides (RC(=O)F) (1960, 1930, 1880 cm⁻¹) as well as a broad complex band in the range 1100–1300 cm⁻¹, corresponding to CF₂ stretching absorptions in several fluorinated degradation products. A further band at 1790 cm⁻¹, attributed to $-\text{CF}_2\text{CF}_2-$ [44], is also present at high temperatures.

A hydrogen fluoride (HF) band with rotational structure centred around \sim 3900 cm⁻¹ is already present at 335 °C for Nafion® and its composite, but only observable beyond 450 °C for pure ODF oligomer. At higher temperatures, pure ODF displays very clear bands at 1500, 1600, 1735 cm⁻¹, which can be attributed to phenyl isocyanates (PhNC) and phenyl nitriles (PhCN), previously reported in the degradation of aryl oxadiazoles [46] and of other polyoxadiazole-based polymers [47]. The high-temperature degradation of ODF also yields gaseous fluorinated hydrocarbons with absorptions peaks in the range 1000–1300 cm⁻¹.

The evolution profiles for different thermal decomposition products can be obtained by plotting the absorbance (normalized by the residual solid sample mass at each point) as a function of temperature, for absorptions at relevant infrared frequencies. Fig. 7 shows the decomposition profiles at wavenumbers 1022, 1230, 1330 and 4040 cm⁻¹, indicative of the evolution of SiF₄/CF₃CFCF₂, RCF₂R', SO₂ and HF respectively.

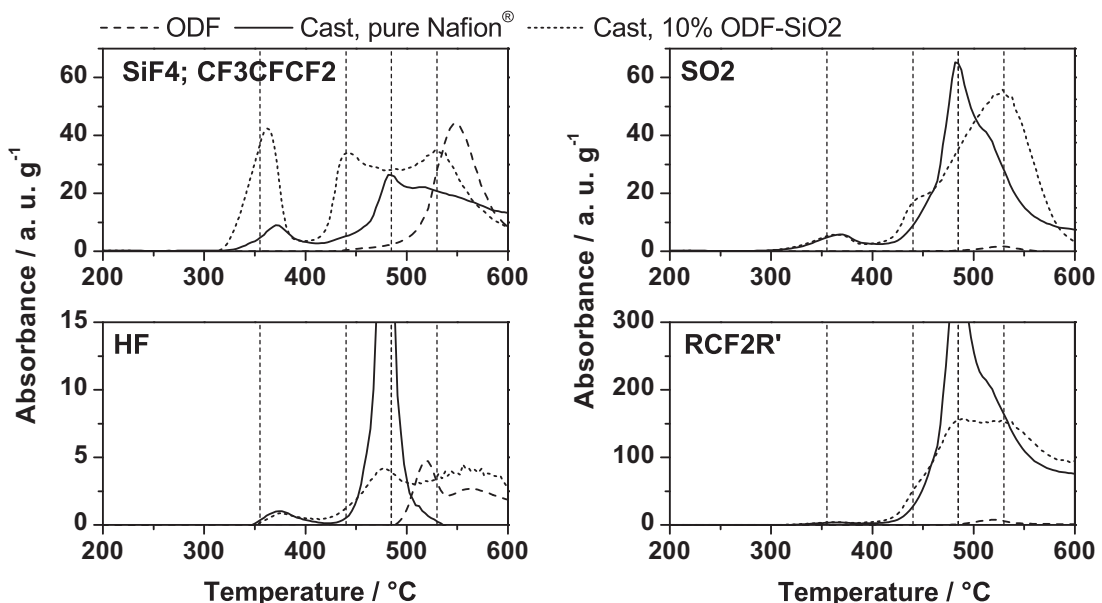


Fig. 7. Thermal decomposition profiles at wavenumbers 1022 (SiF₄; CF₃–CF=CF₂), 1230 (RCF₂R'), 1330 (SO₂) and 4040 cm⁻¹ (HF), for solvent-cast pure Nafion®, telechelic oligomer ODF, and the solvent-cast composite with 10 wt.% ODF-SiO₂. The vertical lines mark the temperatures 335, 440, 485 and 530 °C, for which the full spectra are shown elsewhere in this paper.

Wilkie et al. [48] proposed a degradation mechanism for Nafion® involving an initial cleavage of the C–S bond, resulting in a carbon-based radical and a SO₃H radical. The latter breaks down into SO₂ and an OH radical, while the former suffers further degradation. In agreement with observations by Deng et al. [44] for sol–gel synthesized SiO₂–Nafion® composites, the highest SO₂ profile is obtained for pure Nafion®, as expected from the greater content of sulfonic acid groups. For both Nafion® and its composite, the profile for SO₂ corresponds directly with the thermogram derivative peaks from Fig. 6. Two broad peaks are clearly distinguishable, confirming the presence of –SO₃H groups in at least two different chemical environments. The first peak, with maximum around 365 °C, can be modelled by a single Gaussian, and can be assigned to the –SO₃H in the dry Nafion® matrix. Sulfonic acid groups associated in clusters, are stabilized by strong interactions, and would start to decompose at higher temperatures, explaining the further complex peak in the SO₂ evolution profile. For the composite, reduced mobility due to the presence of nanoparticles is also a stabilizing factor, and allows a fraction of the matrix sulfonic acid groups to tolerate higher temperatures, and thus contribute to the second SO₂ evolution peak.

SiF₄ is produced by reaction between the evolved HF, and SiO₂ present in the filler nanoparticles (4HF + SiO₂ → SiF₄ + 2H₂O) [44]. Wilkie et al. assigned the absorption band at 1022 (1030) cm^{−1} to SiF₄. For the decomposition products of pure Nafion®, they attributed this band to the quartz walls of their TGA sample tube. While our setup contains no quartz parts, we nevertheless observed this absorption during the decomposition of pure Nafion® samples. Hexafluoropropene (CF₃–CF=CF₂), which also absorbs strongly at this wavelength [49], was proposed as a thermal degradation product by Samms et al. [50]. It is generated through an anionic decomposition mechanism, and its presence points to concurrent radical and anionic mechanisms in the thermal decomposition of Nafion®. Starting towards 500 °C, the degradation products of the ODF oligomer show a strong absorption band at this wavelength as well.

As shown in Fig. 7, both for Nafion® and its composite, there are two main SiF₄/CF₃CFCF₂ and HF evolution steps, corresponding to the TGA degradation steps II and III. This behaviour, parallel to the SO₂ evolution, indicates that the sulfonic acid group degradation is always accompanied by some backbone degradation. This is corroborated by the close similarity between the SO₂ and the RCF₂R' evolution profiles. The HF profile corresponds to the portion of that gas that has not reacted with SiO₂ in the system. Consequently, there is a “delay” between the two profiles, with the SiO₂ being evidenced at lower temperatures, as initially all generated HF reacts before it can be detected. The presence of silicon oxide available for reaction in the composite membrane results in both an earlier start and a much higher magnitude for each of the decomposition steps, in comparison to pure Nafion®. At even higher temperatures, the decomposition of the oligomer “shells” results in a clear second maximum at 530 °C for the composite's SiF₄/CF₃CFCF₂ evolution profile.

3.4.3. DSC

Fig. 8 shows differential scanning calorimetry results for the dry composites. A first run, not shown in the figure, was carried out from room temperature to 150 °C at a heating rate of 10 °C min^{−1}, in order to eliminate adsorbed water and to impose a similar thermal history across all samples. Subsequently, the sample was cooled down to –150 °C at 30 °C min^{−1}, and finally a second run at 10 °C min^{−1} was performed up to 280 °C.

A weak transition (not shown in the figure) is observable around –110 °C for the pure cast Nafion® membrane. Corti et al. [41] have assigned this transition to the gamma relaxation

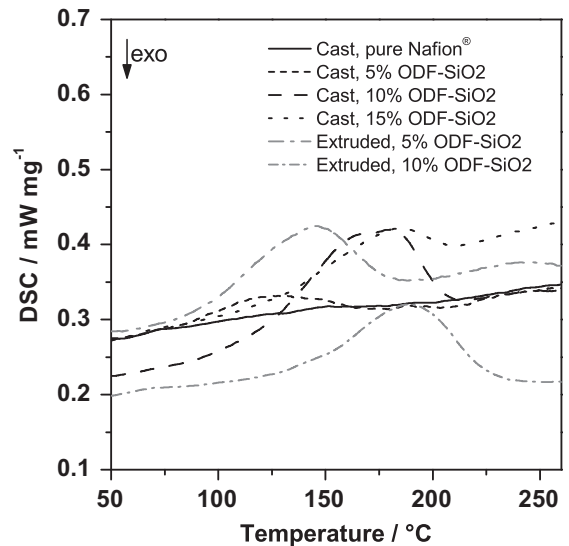


Fig. 8. DSC curves (2nd run) for solvent-cast and extruded Nafion® composites studied in this work, obtained at 10 °C min^{−1}. The first run from room temperature to 150 °C is not shown.

observed in dynamic mechanical studies [51], attributed to motion of the Nafion® backbone. This transition is almost undetectable in the composite membranes, as would be expected from reduced matrix mobility caused by the highly dispersed ODF-SiO₂ nanoparticles.

For all our samples, the first heating up to 150 °C was enough to eliminate most of the freezable water, resulting in the absence of any significant water melting peak [52,53] around 0 °C. In the case of pure cast Nafion®, the pre-heating run was also sufficient to eliminate all water trapped in the ionic clusters (non-freezable water), as evidenced by the absence of a peak [41] in the range 100–200 °C, in the second run. The enhanced water-retention in the composite membranes is substantiated by the endothermic peak at temperatures above 100 °C also in the second run. Increasing the amount of ODF-SiO₂ filler results both in an increased area and a shift to higher temperatures in this peak, in agreement with the observations of Chen et al. [54] for silica-Nafion® composites. Mathematical decomposition of this peak reveals two Gaussian components: if the lower temperature component (Ia) can be assigned to the ionic cluster-bonded water in Nafion®, then the higher temperature component (Ib) probably arises from water more strongly retained by the filler particles. Table S2, in the Supplementary Materials shows the peak temperatures for the Gaussian components of this desorption peak.

3.5. Fuel cell performance evaluation

Fig. S2 in the Supplementary Materials shows typical fuel cell polarization curves of single cells with solvent-cast and extruded 5 and 10 wt.% ODF-silica Nafion® composite membranes. Fuel cell performance of both extruded and solvent cast composite membranes decreases with decreasing the relative humidity. The highest power densities achieved for 5 wt.% and 10 wt.% solvent-cast films are 0.97 and 1.05 W cm^{−2} respectively, while for 5 and 10 wt.% extruded, the highest values are 0.88 and 0.84 W cm^{−2} respectively. The power density for all the membranes decreased significantly as the humidity was lowered to 34%. The humidity affects not only membrane conductivity, but also reactant (O₂ and H₂) partial pressures, and consequently the fuel cell reaction thermodynamics and kinetics [55].

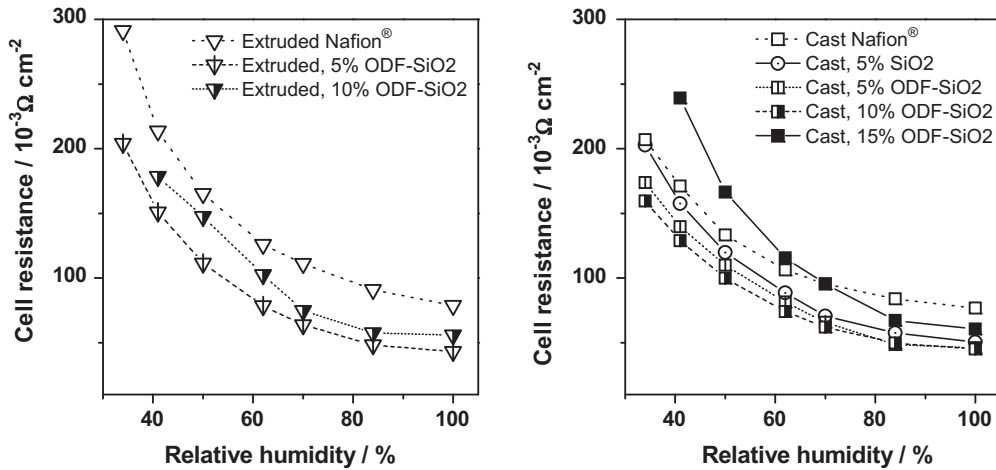


Fig. 9. Fuel cell resistance at 1 A cm^{-2} , for extruded and solvent-cast Nafion® and composite membranes at increasing relative humidities.

Better performance is observed for solvent-cast composite membranes, compared to extruded composites with the same functionalized filler loading. This behaviour can be correlated to the evolution in conductivity values, and probably explained by unavailability, under fuel cell operating conditions, of filler-grafted exchange functions for membranes with poor dispersion. While for the extruded composite membranes the performance peaks at 5 wt.% loading, for the solvent-cast composites the performance continues to improve towards 10 wt.% loading, as the introduced silica-attached sulfonate groups are still available for proton conduction and hence compensating for the missing polymer matrix.

Fig. 9 and Supplementary Materials, Fig. S3 show respectively the fuel cell resistance and voltage values for cells assembled with Nafion® and composite membranes, after 1 h of operation at 1 A cm^{-2} . The cell resistance comprises the contributions from the membrane, the electrodes and the membrane–electrode interfaces, as well as the terminal connections. In order to achieve high fuel cell performance, the cell resistance must be as low as possible. The cell voltage is related to the resistance by Ohm's law, a lower resistance giving a higher cell voltage and consequently a higher power density for a given current density. For both extruded and cast membranes, cell resistance is diminished by the addition of fillers: even the solvent-cast membrane containing 5 wt.% of non-functionalized silica shows lower resistance (higher voltage) values than pure cast Nafion®. A reduced thickness expansion due to reinforcement is most likely the main reason behind this improvement. This beneficial effect is however counteracted at high loadings, as the loss of sulfonated matrix becomes more significant. The lowest resistances (highest voltages) are obtained for 10 wt.% ODF-silica loadings, in the case of solvent cast membranes. For extruded membranes, the optimal composition is 5 wt.%, due to the previously mentioned difference in filler dispersion within the matrix.

3.5.1. Hydrogen crossover

Fig. S4 in the Supplementary Materials shows the hydrogen crossover for the composite membranes in the relative humidity range 34–100%. A slight decrease is observed at high RH values (lower temperature), due mainly to the corresponding temperature reduction in our test conditions, as expected from reports in the literature relating crossover to cell temperature [56,57].

The measured hydrogen crossover was higher for all composite membranes than for pure Nafion®, though the crossover values for composites with different loadings were not significantly different. Cong et al. [58] have proposed the existence of porosity at the particle–matrix interface to explain the permeability increase in

silica-polymer composites. In our case, this would result in reduced crossover for membranes with higher loadings, due to the diminished particle–matrix interface area. However, as agglomeration increases, the intra-aggregate porosity might compensate for this effect, resulting in similar permeabilities for composites with high and low particle contents. An improved compatibilizing agent would be required for better affinity between the particles and the matrix, which in turn would decrease both interfacial porosity and agglomeration, thus reducing hydrogen crossover.

A higher hydrogen crossover was observed for extruded composite membranes. For example at 100% RH the hydrogen crossover of solvent-cast 5 wt.% ODF-silica composite membranes was 5 mA cm^{-2} while that of extruded membranes was 6 mA cm^{-2} . Nevertheless, the crossover increase from the pure polymer to the composite membranes was similar for cast and extruded films (around $3\text{--}4 \text{ mA cm}^{-2}$).

4. Conclusions

A series of Nafion® composite membranes were prepared with silica nanoparticles functionalized with fluorinated oxadiazole oligomers. Both solvent-cast and extruded membranes were obtained with increasing nanoparticle contents, and characterized in order to evaluate their suitability for fuel cell application.

In general, the inclusion of nanoparticles proved beneficial, mainly due to a reinforcement effect and an improvement in water retention. Moreover, due to their higher affinity for the matrix, the functionalized nanoparticles performed better than the pristine silica particles. For the same filler loading, better nanoparticle dispersion was achieved for solvent-cast membranes, which in turn resulted in higher proton conductivity, and thus better fuel cell performance. Nevertheless, larger aggregates are observable for cast membranes at loadings above 5 wt.%.

As particle agglomeration reduces both the reinforcement efficiency and the availability of particle-bonded exchange functions for proton conduction, an optimum nanoparticle content is attained, after which the physicochemical properties of the composites start to degrade again. Best fuel cell performance was obtained for membranes loaded with 10 wt.% ODF-functionalized silica for solvent cast membranes, while the optimal loading was 5 wt.% for the extruded composites.

The composite membranes showed excellent thermal stability, allowing for operation in medium temperature PEM fuel cells. Hydrogen crossover, however, was higher for the composites than for pure Nafion® membranes, possibly due to porosity resulting

from suboptimal particle-matrix compatibility. Even though the fuel cell performance of these composite membranes decreased with decreasing the relative humidity, good performance values were still obtained at 34% RH and 90 °C.

Acknowledgements

The authors would like to thank S. Neumann and Dr. T. Emmler for their contribution to the SEM, and thermal characterizations; F. Vachon, N. Raymond, and P. Le Marquand for their contribution to membrane and MEA processing and characterization. The authors gratefully acknowledge the funding provided by the NRC-Helmholtz Association Cooperation project on MEAs for high temperature fuel cells. Finally, the authors would like to acknowledge the editor's insightful comments.

Appendix A. Supplementary data

Supplementary data related to this article can be found at <http://dx.doi.org/10.1016/j.jpowsour.2013.01.178>.

References

- [1] S.J. Hamrock, M.A. Yandrasits, *J. Macromol. Sci. Polym. Rev.* 46 (2006) 219–244.
- [2] M.Y. Kariduraganavar, R.K. Nagarale, A.A. Kittur, S.S. Kulkarni, *Desalination* 197 (2006) 225–246.
- [3] B. Smitha, S. Sridhar, A.A. Khan, *J. Membr. Sci.* 259 (2005) 10–26.
- [4] M.A. Hickner, H. Ghassemi, Y.S. Kim, B.R. Einsla, J.E. McGrath, *Chem. Rev.* 104 (2004) 4587–4612.
- [5] J.A. Kerres, *J. Membr. Sci.* 185 (2001) 3–27.
- [6] J. Zhang, Z. Xie, J. Zhang, Y. Tang, C. Song, T. Navessin, Z. Shi, D. Song, H. Wang, D.P. Wilkinson, Z.-S. Liu, S. Holdcroft, *J. Power Sources* 160 (2006) 872–891.
- [7] A.-C. Dupuis, *Prog. Mater. Sci.* 56 (2011) 289–327.
- [8] J. Peron, A. Mani, X. Zhao, D. Edwards, M. Adachi, T. Soboleva, Z. Shi, Z. Xie, T. Navessin, S. Holdcroft, *J. Membr. Sci.* 356 (2010) 44–51.
- [9] Y. Shao, G. Yin, Z. Wang, Y. Gao, *J. Power Sources* 167 (2007) 235–242.
- [10] K.A. Mauritz, R.B. Moore, *Chem. Rev.* 104 (2004) 4535–4586.
- [11] B.P. Tripathi, V.K. Shahi, *Prog. Polym. Sci.* 36 (2011) 945–979.
- [12] C. Laberty-Robert, K. Vallé, F. Pereira, C. Sanchez, *Chem. Soc. Rev.* 40 (2011) 961–1005.
- [13] R.K. Nagarale, W. Shin, P.K. Singh, *Polym. Chem.* 1 (2010) 388.
- [14] S.P. Nunes, in: S.M.J. Zaidi, T. Matsuura (Eds.), *Polymer Membranes for Fuel Cells*, Springer, 2009, pp. 223–234.
- [15] D.J. Jones, J. Rozière, *Adv. Polym. Sci.* 215 (2008) 219–264.
- [16] A.M. Herring, *J. Macromol. Sci. Polym. Rev.* 46 (2006) 245–296.
- [17] S. Licoccia, E. Traversa, *J. Power Sources* 159 (2006) 12–20.
- [18] G. Alberti, M. Casciola, *Annu. Rev. Mater. Res.* 33 (2003) 129–154.
- [19] D.J. Jones, J. Rozière, in: W. Vielstich (Ed.), *Handbook of Fuel Cells: Fundamentals, Technology, Applications*, Wiley, 2003, pp. 447–455.
- [20] R. Gosalawit, S. Chirachanchai, S. Shishatskiy, S.P. Nunes, *J. Membr. Sci.* 323 (2008) 337–346.
- [21] C.H. Rhee, H.K. Kim, H. Chang, J.S. Lee, *Chem. Mater.* 17 (2005) 1691–1697.
- [22] G. Alberti, M. Casciola, in: K.V. Peinemann, S.P. Nunes (Eds.), *Membranes for Energy Conversion* (2008), pp. 97–122.
- [23] A.S. Aricò, V. Baglio, V. Antonucci, in: K.V. Peinemann, S.P. Nunes (Eds.), *Membranes for Energy Conversion* (2008), pp. 123–167.
- [24] A. Saccà, A. Carbone, E. Passalacqua, A. D'Epifanio, S. Licoccia, E. Traversa, E. Sala, F. Traini, R. Ornelas, *J. Power Sources* 152 (2005) 16–21.
- [25] C. Sanchez, F. Ribot, B. Lebeau, *J. Mater. Chem.* 9 (1999) 35–44.
- [26] M.L. Di Vona, Z. Ahmed, S. Bellitto, A. Lenci, E. Traversa, S. Licoccia, *J. Membr. Sci.* 296 (2007) 156–161.
- [27] A.K. Sahu, G. Selvarani, S. Pitchumani, P. Sridhar, A.K. Shukla, *J. Electrochem. Soc.* 154 (2007) B123–B132.
- [28] B. Baradie, J.P. Dodelet, D. Guay, *J. Electroanal. Chem.* 489 (2000) 101–105.
- [29] K.A. Mauritz, I.D. Stefanithis, S.V. Davis, R.W. Scheetz, R.K. Pope, G.L. Wilkes, H. Huang, *J. Appl. Polym. Sci.* 55 (1995) 181–190.
- [30] G. Gnana Kumar, A.R. Kim, K. Suk Nahm, R. Elizabeth, *Int. J. Hydrogen Energy* 34 (2009) 9788–9794.
- [31] H. Wang, B.A. Holmberg, L. Huang, Z. Wang, A. Mitra, J.M. Norbeck, Y. Yan, *J. Mater. Chem.* 12 (2002) 834–837.
- [32] R.R. Abbaraju, N. Dasgupta, A.V. Virkar, *J. Electrochem. Soc.* 155 (2008) B1307–B1313.
- [33] D. Gomes, S.P. Nunes, *J. Membr. Sci.* 321 (2008) 114–122.
- [34] D. Gomes, R. Marschall, S.P. Nunes, M. Wark, *J. Membr. Sci.* 322 (2008) 406–415.
- [35] D. Gomes, J. Roeder, M.L. Ponce, S.P. Nunes, *J. Membr. Sci.* 295 (2007) 121–129.
- [36] D. Gomes, S.P. Nunes, J. Carlos Pinto, C. Borges, *Polymer* 44 (2003) 3633–3639.
- [37] D. Gomes, I. Buder, S.P. Nunes, *Desalination* 199 (2006) 274–276.
- [38] J. Lin, J.K. Lee, M. Kellner, R. Wycisk, P.N. Pintauro, *J. Electrochem. Soc.* 153 (2006) A1325–A1331.
- [39] E. du Pont de Nemours and Company, Technical Information Sheet NAE302 (2002).
- [40] A. Mokrini, M.A. Huneault, Z. Shi, Z. Xie, S. Holdcroft, *J. Membr. Sci.* 325 (2008) 749–757.
- [41] H.R. Corti, F. Nores-Pondal, M. Pilar Buera, *J. Power Sources* 161 (2006) 799–805.
- [42] S.K. Tiwari, S.K. Nema, Y.K. Agarwal, *Thermochim. Acta* 317 (1998) 175–182.
- [43] J. Surowiec, R. Bogoczek, *J. Therm. Anal.* 33 (1988) 1097–1102.
- [44] Q. Deng, C.A. Wilkie, R.B. Moore, K.A. Mauritz, *Polymer* 39 (1998) 5961–5972.
- [45] L.G. Lage, P.G. Delgado, Y. Kawano, *J. Therm. Anal. Calorim.* 75 (2004) 521–530.
- [46] R. Frański, G. Schroeder, V. Rybachenko, O.P. Szwajka, *Rapid Commun. Mass Spectrom.* 16 (2002) 390–395.
- [47] M.L. Ponce, J. Roeder, D. Gomes, S.P. Nunes, *Asia-Pacific J. Chem. Eng.* 5 (2010) 235–241.
- [48] C.A. Wilkie, J.R. Thomsen, M.L. Mittleman, *J. Appl. Polym. Sci.* 42 (1991) 901–909.
- [49] M. Mashino, Y. Ninomiya, M. Kawasaki, T.J. Wallington, M.D. Hurley, *J. Phys. Chem. A* 104 (2000) 7255–7260.
- [50] S.R. Samms, S. Wasmus, R.F. Savinell, *J. Electrochem. Soc.* 143 (1996) 1498–1504.
- [51] T. Kyu, M. Hashiyama, A. Eisenberg, *Can. J. Chem.* 61 (1983) 680–687.
- [52] K. Asaka, N. Fujiwara, K. Oguro, K. Onishi, S. Sewa, *J. Electroanal. Chem.* 505 (2001) 24–32.
- [53] L. Gomes Lage, P. Gomes Delgado, Y. Kawano, *Eur. Polym. J.* 40 (2004) 1309–1316.
- [54] C.-Y. Chen, J.I. Garnica-Rodriguez, M.C. Duke, R.F.D. Costa, A.L. Dicks, J.C.D. da Costa, *J. Power Sources* 166 (2007) 324–330.
- [55] J. Zhang, Y. Tang, C. Song, Z. Xia, H. Li, H. Wang, J. Zhang, *Electrochim. Acta* 53 (2008) 5315–5321.
- [56] X. Cheng, J. Zhang, Y. Tang, C. Song, J. Shen, D. Song, J. Zhang, *J. Power Sources* 167 (2007) 25–31.
- [57] J. Zhang, Y. Tang, C. Song, J. Zhang, H. Wang, *J. Power Sources* 163 (2006) 532–537.
- [58] H. Cong, X. Hu, M. Radosz, Y. Shen, *Ind. Eng. Chem. Res.* 46 (2007) 2567–2575.